# Geometry-Specific Heterogeneity of the Apparent Diffusion Rate of Materials Inside Sperm Cells

Daisuke Takao[†‡] and Shinji Kamimura[§*]

[†]Department of Life Sciences, Graduate School of Arts and Sciences, The University of Tokyo, Tokyo, Japan; [‡]Laboratory for Spatiotemporal Regulations, National Institute for Basic Biology, Aichi, Japan; and [§]Department of Biological Sciences, Faculty of Science and Engineering, Chuo University, Tokyo, Japan

ABSTRACT In sea urchin spermatozoa, the energy source powering flagellar motion is provided as ATP produced by mitochondria located at the proximal ends of flagella. However, the bottleneck structure between the sperm head and the flagellar tail seems to restrict the free entry of ATP from mitochondria into the tail region. To test this possibility, we investigated the diffusion properties in sperm cells using fluorescence recovery after photobleaching. We found that the rate of fluorescence recovery in the head region was ~10% of that observed in the flagellar tail regions. We also found that, even within the tail region, rates varied depending on location, i.e., rates were slower at the more distal regions. Using computational analysis, the rate heterogeneity was shown to be caused mainly by the geometry of the sperm structure, even if little or no difference in diffusion rates through the neck region was assumed. Therefore, we concluded that materials such as ATP would generally diffuse freely between the heads and the flagella of sperm cells. We believe these findings regarding the diffusion properties inside spermatozoa provide further insights into material transportation and chemical signaling inside eukaryotic cilia and flagella.

## INTRODUCTION

In sea urchin spermatozoa, the energy required for flagellar motility has simply been assumed to be provided by the diffusion of ATP or creatine phosphate in flagella. This model has been suggested previously by simulation (1) and by our previous study to determine the diffusion coefficients in flagella (2). Lacking direct evidence, we have generally believed that ATP produced in mitochondria should diffuse freely through the neck regions into the sperm tails because sufficient ATP seems to be provided to support continuous flagellar beating. However, in contrast to mammalian sperm, with mitochondria contained in a long flagellar mid-piece, the mitochondria of sea-urchin sperm cells are located in the posterior ends of the heads, i.e., in the cell bodies. Thus, bottleneck effects at the connections between the heads and the flagella, if any should exist, could be an obstacle to free ATP supply from mitochondria to the flagellum. This possibility is also supported by evidence from electron microscopy observations in which the neck region between the head and the flagellum was shown to be densely packed in mammalian sperm (3) and *Chlamydomonas* flagella (4). In addition, the presence of diffusion barriers has been reported in the plasma membrane of mammalian sperm (5–7). Such evidence suggests that there could be an intracellular diffusion barrier around the neck region.

Although recent detailed information regarding the active intraflagellar transport systems along cilia and flagella showed the critical roles of such systems in the structural and functional maintenance of axonemes (8,9), another possible path of material diffusion beyond the neck region has not been described in detail. In either case where such an active or passive process is included in the transportation system, the possibility that the obstacles and the molecular crowding conditions inside sperm cells could modify the rate of ATP supply should be tested to understand the exact ATP energetics in spermatozoa.

Along with the ATP energetics of sperm motility, intracellular material diffusion is also a crucial point when we are going to clarify the precise kinetics of chemical signaling inside cilia and flagella. Because recent studies have shown that some ion channels and ligand receptors required for many cell functions are located not on cell bodies but on ciliary shafts (10,11), we expect that detailed investigations into the diffusion phenomenon in cilia and flagella should give us new insights into the efficiency of chemical signaling and help us to clarify the sensing mechanisms by primary cilia.

In this study, to test the possibility of diffusion restriction inside sperm cells, we investigated the molecular mobility through the neck regions as well as inside sperm tails. First, fluorescence recovery after photobleaching (FRAP) experiments, in which heads or various regions along flagella were photobleached, were executed in sperm loaded with fluorescent probes. In this approach, we observed the heterogeneities of apparent diffusion rates within sperm cells, which had been expected to reflect the geometric effects of sperm architecture, as well as to indicate the existence of a diffusion barrier between head and flagellum, if one should exist. Second, to investigate the actual cause of the heterogeneity

*Submitted September 22, 2009, and accepted for publication December 24, 2009.*

*Correspondence: kam@myad.jp



Editor: Michael E. Fisher.



0006-3495/10/04/1582/7 $2.00

doi: 10.1016/j.bpj.2009.12.4314

of apparent diffusivity, we constructed a computer-simulation model in which the sperm cell was assumed to be constructed by connected cubic segments. The model showed that the three-dimensional shape of a sperm cell can be a primary factor that affects apparent diffusivity regardless of pure diffusion coefficients, suggesting that one should be careful to discuss diffusivity from FRAP experiments. Consequently, the results obtained from these approaches indicated there would be no apparent diffusion barrier in the neck region, at least for the fluorescent probes we examined. Molecular diffusivities in the neck region may be hardly restricted, at least for small molecules such as ATP.

## MATERIALS AND METHODS

### Materials

Chemicals were purchased from the following suppliers unless otherwise stated: Wako (Osaka, Japan), Sigma-Aldrich Japan (Tokyo, Japan), or Dojindo (Kumamoto, Japan). Fluorescent probes (carboxyfluorescein, Oregon Green, calcein, fluorescein-dextran) were obtained from Invitrogen (Carlsbad, CA). Sea urchin sperm (*Pseudocentrotus depressus* or *Anthocidaris crassispina*) were obtained by intracoelomic injection of 0.5 M KCl. Spawned sperm was collected and stored without dilution (dry sperm) at 4°C until the time of use. Experimental results obtained with both sea urchin species were almost indistinguishable from one another, and all the data from both species were treated all together. A solution containing 225 mM K-gluconate, 225 mM mannitol, 20 mM NaCl, 20 mM $MgCl_2$, 10 mM HEPES (pH 7), and 0.5% (w/v) BSA was used for the experimental medium (12,13). Under these conditions, almost all of the sea urchin spermatozoa were nonmotile, and cells that had been adhered onto glass surfaces were used for the experiments.

### Fluorescence loading and FRAP analysis

All fluorescent probes were loaded into sea urchin sperm cells by the single-cell electroporation technique (13,14). In short, in this loading method, fluorescent probes are loaded from a glass micropipette into cells by exerting electric pulses between electrodes in the micropipette and in the bath solution, i.e., electroporation is executed locally at the single-cell level. The glass micropipettes had a similar shape to those of patch clamps, with a tip inner diameter of ~1 $\mu$m. They contained 200 $\mu$M of probes in distilled water. The parameters for electric pulses were as follows: a driving voltage of 100 V; current monitored by a register connected to a reference electrode of ~1 $\mu$A; a pulse frequency and duration of 200 Hz and 3 ms, respectively; and a pulse train duration of 0.5–3 s (100–600 pulses). Subsequent FRAP analysis was also executed as described previously (2).

### Simulation model

To simulate the diffusional dynamics inside the sperm cell, we constructed a three-dimensional model for computer simulation (Fig. 1). In the model, the spermatozoon is composed of cubic segments, where materials diffuse between neighboring segments with diffusion coefficients defined in each boundary: $D_H$, $D_N$, and $D_F$, in the head, neck (segment at the basal end of flagellum), and flagellar segments, respectively. The model spermatozoon used here is finite in length. When the concentration of materials in a given segment of the sperm model, $s_{x,y,z}$, at time $t$ is denoted as $c_{x,y,z}(t)$, the differential equation

$$\partial c_{x,y,z}(t)/\partial t = \frac{D_H}{\Delta s^2}\big(c_{x-1,y,z}(t) - 2c_{x,y,z}(t) + c_{x+1,y,z}(t) + c_{x,y-1,z}(t) - 2c_{x,y,z}(t) + c_{x,y+1,z}(t) + c_{x,y,z-1}(t) - 2c_{x,y,z}(t) + c_{x,y,z+1}(t)\big), \quad (1)$$

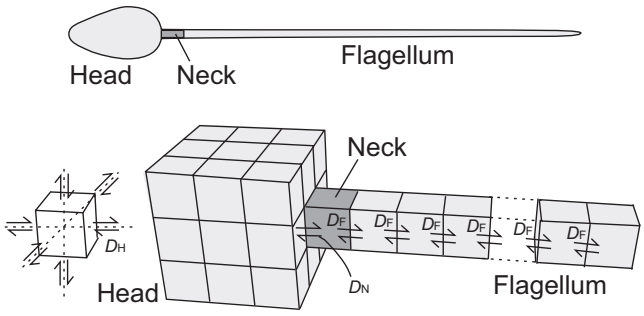


FIGURE 1 Schematic drawing of the sperm cell model constructed in this study for computer simulation. In this model, the spermatozoon is made of assembled cubic segments and materials can diffuse between the adjacent segments. Note that the flagellum is made of a single line of segments (one-dimensional) whereas the head is a stack of segments (three-dimensional).

is derived (based on Fall et al. (15)) for three-dimensional diffusion in the head, where $D_H$ is the diffusion coefficient in the head segments and $\Delta s$ is the length of each segment (1 $\mu$m in this study). In this equation, the rate of $c_{x,y,z}(t)$ change is expressed as a result of efflux from the segment $s_{x,y,z}$ as well as influxes from the adjacent segments $s_{x\pm1,y,z}$, $s_{x,y\pm1,z}$, and $s_{x,y,z\pm1}$, which depend on $D_H$ and concentration gradients. The head is assumed to be isolated from the surrounding medium to execute the simulation of diffusion inside the restricted finite system, i.e., a reflective boundary condition was assumed and no influx or efflux occurs beyond the surface boundaries of the head. For example, if the segment $s_{-4,0,0}$ is assigned as a surface segment of the head (in this case, segments of $-4 \le x \le 0$ correspond to the head), $s_{-5,0,0}$ does not exist and the segments adjacent to $s_{-4,0,0}$ are $s_{-3,0,0}$, $s_{-4,\pm1,0}$, and $s_{-4,0,\pm1}$.

On the other hand, we regarded the flagellum as a single, one-dimensional array of segments along the $x$ axis ($y = z = 0$) with no influx or efflux across the distal end of the flagellum (reflective boundary). The differential equation

$$\begin{aligned}\partial c_1(t)/\partial t &= \frac{D_N}{\Delta s^2}(c_0(t) - c_1(t)) + \frac{D_F}{\Delta s^2}(c_2(t) - c_1(t)) \quad x = 1 \text{ (neck segment)},\\ \partial c_x(t)/\partial t &= \frac{D_F}{\Delta s^2}(c_{x-1}(t) - 2c_x(t) + c_{x+1}(t)) \quad 2 \le x < L,\\ \partial c_L(t)/\partial t &= \frac{D_F}{\Delta s^2}(c_{L-1}(t) - c_L(t)) \quad x = L \text{ (tip segment)},\end{aligned} \quad (2)$$

is similarly derived for the flagellum, where $D_N$ and $D_F$ are diffusion coefficients in the boundary between the head and the flagellum, and inside the flagellum, respectively, and $L$ is the flagellar length (set to 40 $\mu$m in this study). The most basal and distal ends of the flagellum are denoted as neck and tip segments, respectively. When segments with $1 \le x \le L$ are assigned to the flagellum, as in Eq. 2, segments with $x \le 0$ including $s_{0,0,0}$ are assigned to the head region (simultaneous equations for simulating the diffusion inside the entire spermatozoon were formed with Eq. 1 and Eq. 2).

In the case of photobleaching of the head region, the initial concentration values, $c_{x,y,z}(0)$, were set to be uniform in the head segments, whereas no photobleaching occurs in the neck and flagellar segments, e.g., $c_{x,y,z}(0) =$ 0.4, 1.0, and 1.0, in the head, neck, and flagellar segments, respectively. On the other hand, in the case when a photobleaching laser beam with a Gaussian profile was focused on segment $s_{,B,y,z}$ along the flagellum, $c_x(0)$ in the flagellum ($y = z = 0$) is defined as

$$c_x(0) = C_0\mathrm{Exp}\left[-K\,\mathrm{Exp}\left[-2\{(x-B)\Delta s\}^2/\omega^2\right]\right], \quad (3)$$

where $C_0$ is a normalized value of concentration (set to 1.0 in this study), $\omega$ is the laser radius at $1/e^2$, and $K$ is the constant parameter for the depth of photobleaching (based on Eqs. 1–3 in Axelrod et al. (16)). Similar to the previous FRAP experiments, half-recovery rates, $t_{1/2}$, were obtained by fitting the simulated data to the equation (2,17,18)

$$F(t) = \frac{F_0 + F_\infty \times \left(t/t_{1/2}\right)}{1 + \left(t/t_{1/2}\right)}, \quad (4)$$

where $F(t)$ is the fluorescence intensity at time $t$. $F_0$ and $F_\infty$ are the fluorescence intensities immediately and at an infinite time after the photobleaching, respectively. All calculations stated here were executed using programs written with Mathematica (version 6.0, Wolfram Research, Champaign, IL).

## RESULTS

### FRAP in the spermatozoon head

To investigate whether diffusion is restricted in the neck region of sea urchin spermatozoa, we first observed fluorescence recoveries when photobleaching laser beams were directed on the heads of four species of fluorescent probes; fluorescent dyes with a molecular mass comparable to ATP (carboxyfluorescein, Oregon Green, and calcein), and for comparison, a relatively larger species, fluorescein-dextran of MW 3000 (3k-FD), were chosen for probes, with the limitation that the probe species are capable of being incorporated into sperm cells (e.g., at the moment, dextran larger than MW 3000 was not successful in the case of sea urchin spermatozoa).

Because the size of the focused laser beam was comparable to that of the sperm head, the mean fluorescence intensities of the entire head region on recorded images were analyzed. For all of the probe species we examined, we found the fluorescence of the head regions gradually recovered after photobleaching as shown in Fig. 2 *A*. This indicates that these probes are mobile through the neck region. Half-recovery times, $t_{1/2}$, in heads were about one order of magnitude longer in comparison with those inside flagella (Fig. 3). Such slower recovery rates in the heads might suggest the existence of partial restrictions that slow down the rate of free diffusion through the neck region. However, a simple comparison between half-recovery times in the heads and the flagella is not appropriate, because the three-dimensional diffusion of materials in heads could be quite different from that of one-dimensional diffusion inside the flagella of long tubular shapes. During photobleaching at the head region, we also observed reductions of fluorescence intensities of ~50% at the most proximal tail regions ($<$ ~3 $\mu$m from heads). Presumably, this was due to photobleaching side-effects from scattering light from the photobleaching beam directed on the heads, or due to rapid diffusion through the neck regions. Because of the small volume ratio of this proximal region (~1/60, based on Takao and Kamimura (2)) comparing with that of the sperm head, the effect on the rate of fluorescence recovery of the head would have been small. Therefore, this side effect was neglected and we focused instead on the FRAP analysis in the tail region in the following experiments.

### Dependency of recovery rates on the position along the flagellum

To investigate the diffusion properties around the neck region in detail, we then compared fluorescence recovery rates in various positions along the flagella (Fig. 2, *B–D* and Fig. S1 in the Supporting Material). Our first assumption was that sperm geometry should affect recovery rates; at the

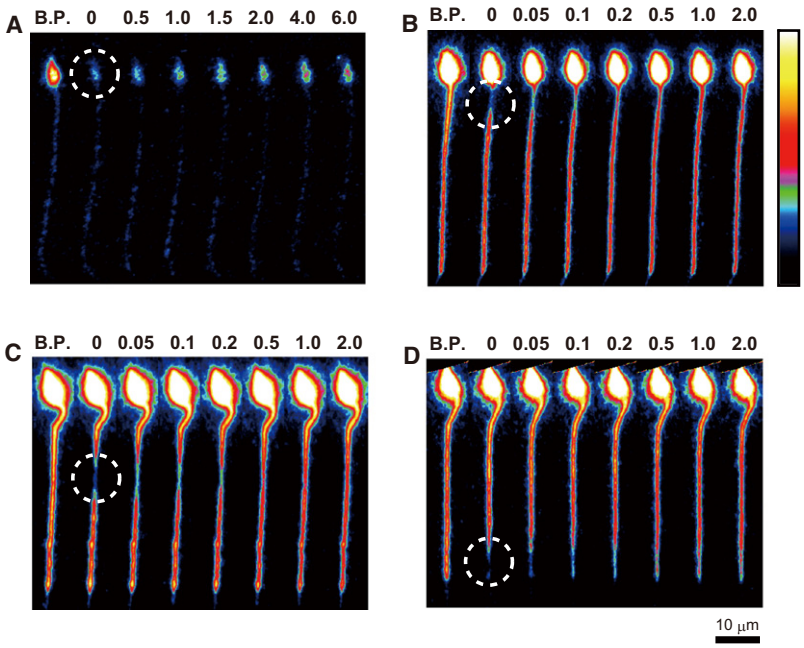


FIGURE 2 Example images of FRAP experiments in spermatozoa loaded with carboxyfluorescein. Each image was obtained by averaging 5 frames (10 ms/frame). The resultant images of brightness maps are displayed in pseudo-color (white is the brightest and black is the faintest) to clarify the details of the photobleached area. The numbers shown above each image indicate the time course after the photobleaching laser pulse was directed (unit: s; B.P. indicates before photobleaching). The broken circles indicate the regions where the photobleaching laser pulses were directed. (*A*) Fluorescence recovery after the head was photobleached. (*B–D*) Cases where photobleaching laser pulses were directed on the (*B*) neck, (*C*) mid, and (*D*) tip in flagella. The depth of photobleaching in example images shown here was twice that for quantitative data analyses to clarify the details of photobleached areas.

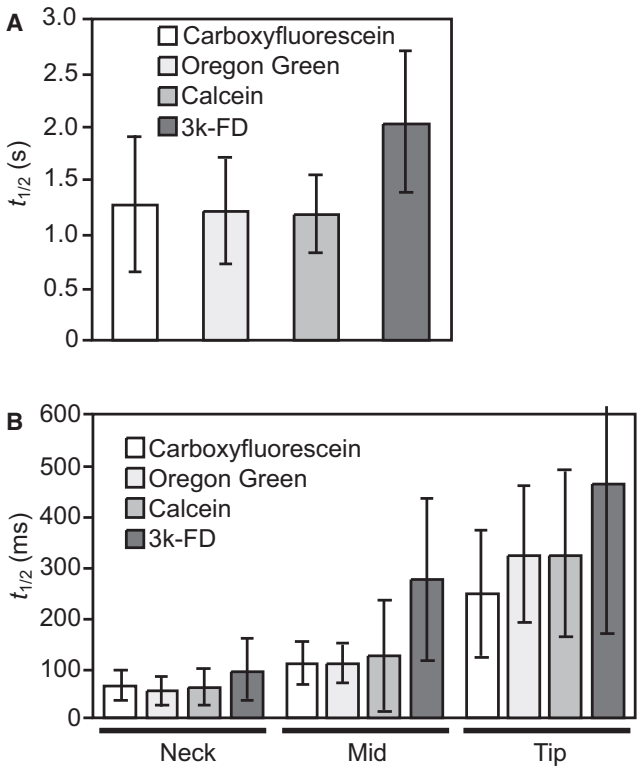


FIGURE 3 Dependency of half-recovery times on the position of photobleaching. The half-recovery times of fluorescence, $t_{1/2}$, obtained in sperm loaded with fluorescent probes are shown. Data obtained in the cases where the head was photobleached (*A*) as well as photobleaching laser pulses directed to the neck, mid, and tip regions in flagellum (*B*) are expressed as mean ± SD ($n = 6$–16).

tip, for example, recovery rates should be slower than those in the mid-region because no influx of unbleached probes from the distal end is expected (single-sided diffusion), whereas there would be an influx from both neighboring regions in the mid-regions (double-sided diffusion). If we could assume that the neck boundary between the head and the flagellum is completely enclosed, (i.e., no diffusion from the head region is permitted) the properties of fluorescence recoveries at the neck should be the same as those observed at the tip. Although this assumption should be incorrect, as we have already demonstrated materials moving through the neck (Fig. 2 *A* and Fig. 3 *A*), analyzing the dependency of recovery rates at positions along flagellum would provide some clues for understanding the actual diffusion properties around the neck.

As shown in Fig. 4, the half-recovery time of carboxyfluorescein was not constant but tended to be longer around the flagellar ends whereas other parameters of $F_0$ and $F_\infty$ were almost the same (Fig. S2). We obtained similar results for all fluorescent probe species, as shown in Fig. 3 *B*, where FRAP analysis was executed in three different regions termed as neck, mid, and tip, which corresponded to the regions within 10 $\mu$m, ~20 $\mu$m, and >30 $\mu$m away from the proximal

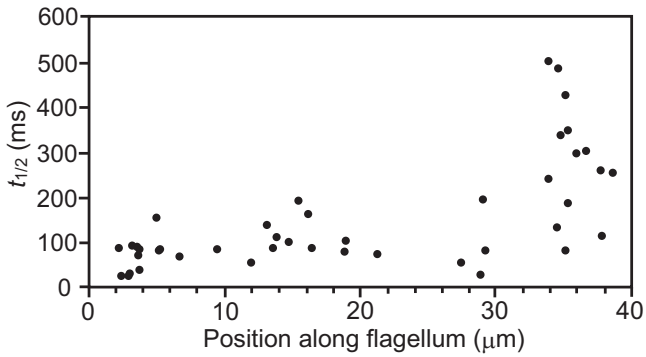


FIGURE 4 The relationship between half-recovery time and position along the flagellum. The fitting parameter of half-recovery time, $t_{1/2}$, is plotted against the position along the flagellum loaded with carboxyfluorescein. Position is expressed as distance from the proximal end of the flagellum.

end of flagellum, respectively (flagellar length is typically ~40 $\mu$m). Examples of typical fluorescence recovery curves of carboxyfluorescein are shown in Fig. S1. In summary, for all fluorescence probes, $t_{1/2}$ was one-third to one-half at the neck and two to three times larger at the tip, in comparison with those at the mid-region. As stated above, the recovery rates were slower at the tip than those at the mid. The obtained recovery rates at the neck were faster than those at any other regions in flagellum.

## Simulation of molecular diffusion in the sperm cell

To explain the observed heterogeneity of recovery rates (Fig. 3 *B*), we constructed a simple model as illustrated in Fig. 1. In this model, the sperm is regarded as a structure of connected cubic segments. The head, composed of stacked segments, is connected to the linearly-aligned segments of the tail region via a neck segment. In this study, the head segments were set to $5 \times 5 \times 7$ ($x \times y \times z$; the flagellum is on the $x$ axis); thus, the number of head segments was 175, whereas that of the flagellum was 40. The head-to-flagellum volume ratio was 4.375:1.0, which is comparable to the previously determined ratio of 4.6:1.0 (2). The head was illustrated as a stack of $3 \times 3 \times 3$ segments in Fig. 1, for simplification. The values of the diffusion coefficients can be individually assigned for each boundary between segments; for practical purposes, we assigned diffusion coefficients for three distinct regions, i.e., head ($D_H$), neck ($D_N$), and flagellum ($D_F$).

Using this model, FRAP experiments in various regions of the flagella were simulated. Half-recovery times, $t_{1/2}$, were calculated over the points along the flagellum with various sets of diffusion parameters, $D_H$, $D_N$, and $D_F$. Examples of calculated $t_{1/2}$ values were plotted over the experimental data points and shown in Fig. 5. In each case, $t_{1/2}$ was found to increase steeply at the tip (Fig. 5, *A–D*). $D_H$ and $D_N$ hardly affected $t_{1/2}$ (Fig. 5, *B* and *C*). However, $D_F$ had a significant influence on $t_{1/2}$ (Fig. 5 *D*).

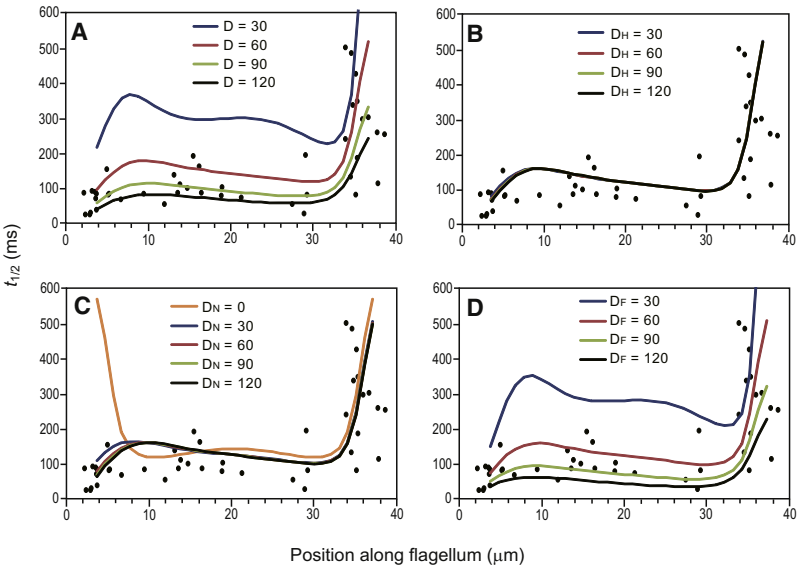


FIGURE 5 Example results obtained from the simulations. The simulated $t_{1/2}$ curves were plotted against the position along the flagellum. The experimental data (*solid circle*) shown in Fig. 4 were superimposed onto each plot. (*A*) Diffusion coefficients in the head ($D_H$), the neck ($D_N$), and the flagellum ($D_F$) were set to the same values. (*B–D*) Variations of each of the three diffusion coefficients, (*B*) $D_H$, (*C*) $D_N$, and (*D*) $D_F$ are shown whereas the other two remain constant (set to 60 $\mu m^2/s$). Color lines are shown online only.

In the case where $D_H$ or $D_N$ was much smaller than $D_F$ (i.e., $D_H$ or $D_N$ was nearly zero), $t_{1/2}$ at the proximal end of the flagellum increased (diffusion was slow) similarly to the distal end. On the other hand, setting $D_H$ and $D_N$ comparable to $D_F$, we could mimic our experimental data well and show a decreased $t_{1/2}$ at the proximal regions (Fig. 5, *B* and *C*). Note that if $D_N$ was set to zero (the boundary between the head and the flagellum was entirely enclosed), the resulting molecular diffusion in the proximal region was the same as that in the tip region (single-sided diffusion). $D_F$ affected $t_{1/2}$ evenly throughout nearly the entire region of the flagellum, thus $D_F$ alone is the primary factor that determines $t_{1/2}$ around the neck region (Fig. 5 *D*). In summary, $D_H$ and $D_N$ locally affected $t_{1/2}$ in the proximal region but their effects were minimal, whereas $D_F$ significantly affected the whole area in the flagellum. When $D_H$ and $D_N$ were comparable to $D_F$ set to 60–80 $\mu m^2/s$, we obtained the smallest residuals between experimental and simulated data (Fig. S3).

## DISCUSSION

In the scope of investigating whether diffusion is restricted in the neck region between the head and the flagellum, we analyzed the FRAP rates of fluorescence probes that had been introduced into sperm cells using a single-cell electroporation technique. An apparent heterogeneity of FRAP rates inside sperm cells was found, and the data we obtained were compared with those from simulated diffusion. The results obtained from the current study can be summarized as follows: i), when fluorescent probes in sperm heads were photobleached, subsequent fluorescence recoveries were observed despite the slower recovery rates compared to those in flagella (Fig. 2 *A*), indicating that, at least the molecules we examined, i.e., carboxyfluorescein, Oregon Green, calcein, and 3k-FD, are able to move through the neck region; ii), the comparison of FRAP rates in the neck, mid, and tip regions (Fig. 2, *B–D*) showed that the obtained half-recovery times, $t_{1/2}$, were smaller at the neck (faster recovery) and larger (slower) at the tip, in comparison to those at the mid (Fig. 3 *B*); and iii), a model constructed to simulate molecular diffusion in sperm cells reproduced the experimental results when little or no restriction of diffusivity at the neck was assumed (Fig. 5).

The larger $t_{1/2}$ at the tips of flagella compared with those in other regions (mid or neck) may be derived from the effect of the tip enclosure. In mid-regions, fluorescent molecules can enter from both the proximal and the distal ends of the photobleached area, whereas, in the tip region, an influx is expected from the proximal side alone, i.e., single-sided diffusion. Tip enclosure may cause a deceleration of the FRAP rates at the tip region. As shown by our model simulations and experimental results (Fig. 5), $t_{1/2}$ is not simply doubled in the case of single-sided diffusion, but was steeply increased at the tip. In our simplified model, no other boundary condition for diffusion was assumed at the distal end except for the closed-end structure, which strongly suggests that the apparent rate of diffusion is under a strong influence from the geometry of the cell shapes. Thus far, such a geometric effect as high as up to a ~5-fold increase in $t_{1/2}$, which we had not expected, has never been shown theoretically or experimentally. Our observations also indicate that the simple effect of the closed tip-end may dramatically affect molecular movements or distribution.

Large deviations in experimentally-obtained $t_{1/2}$ at the tip region would have been partially due to such steep increases of $t_{1/2}$ at the tip. Some variations in full-length flagella, as well as in the end-piece length, of sea-urchin sperm cells would be related as well. Smaller $t_{1/2}$ at the neck region, on the other hand, may be derived from the effects of connections to heads where a three-dimensional, faster spreading of

materials should be allowed. To reproduce our experimental data, the diffusion rate through the neck segment seemed to be similar to those in the mid-region. When considering both experimental and computational analyses, small molecules such as ATP may be highly diffusive through the neck boundary although FRAP rates should be apparently affected by the geometry, i.e., the closed flagellar end and the connection of the flagellum to the three-dimensionally spreading head.

If the diffusion coefficients in the flagellum, $D_F$, are almost the same along the flagellum, as shown in the present model, cell geometry is the primary factor that affects FRAP rates, and thus, apparent diffusion coefficients. This may be the case in real sperm cells. As the axoneme has a uniform 9 + 2 structure along the entire length of the flagella (19,20), the physical environment for material diffusion should be uniform and it is unlikely that the pure diffusion coefficient is heterogeneous along the flagellum. It is also indicated that one should be careful to determine the real diffusion coefficients from the recovery rates obtained in FRAP experiments. As shown in Fig. 5, $t_{1/2}$ was less affected by geometry in the region between 10–30 $\mu$m of the proximal end of a 40-$\mu$m long flagellum. By FRAP analysis around the mid-regions of flagella, we had previously determined the diffusion coefficients of fluorescein derivatives in flagella to be ~60 $\mu m^2/s$ (2). With a $D_F$ value of 60–80 $\mu m^2/s$, regardless of $D_H$ and $D_N$ values, simulated $t_{1/2}$ distributions fit the experimental data well (Fig. 5 and Fig. S3). Therefore, the previous experimental results and the current simulation model are consistent with each other.

These results also provided us further insights into material diffusion in other cells. Recent studies on ciliopathy have shown that the related ion channels or chemical receptors are located not on the surface of cell bodies but along the shaft of primary cilia (10,11). We may simply expect any sensory mechanisms to be located on ciliary projections for effective sensing of extracellular chemicals without any specific evaluations or theoretical background. However, this study suggests strongly that the sensors are required to be located on cilia for quick intracellular signaling. Comparing the cell surface location, ciliary sensors seem to be promising the quick increase and decrease of chemical signals just beneath the ciliary membrane. It is suggested that cell geometry and its effects on the material diffusion would be crucial to understand the kinetics of intracellular pathways of signal transduction.

At present, we have concluded that, at least for small molecules such as ATP, molecular diffusion is hardly restricted in the neck of sea urchin spermatozoa, as mentioned above. It is possible, however, that diffusivity at the neck depends on the molecular species. In somatic cells, structures called transition fibers are known to be located in the boundaries between cilia and cell bodies, and these fibers have been considered to function as molecular filters (8,9,21). In addition, specific localization of proteins and signaling pathways and selective transportation of materials by intraflagellar transport systems have been reported in primary cilia (11,22,23). Such evidence indicates that the mobility of macromolecules such as proteins is restricted within cilia, whereas smaller ions or molecules, such as $Ca^{2+}$ ions and ATP, seem to freely pass through the boundary between cilia and cell bodies (24,25). Therefore, despite the lack of evidence for an obvious diffusion barrier in the fluorescent probes examined here, it remains possible that such a filtering mechanism exists in the neck of spermatozoa. From this point of view, it is worthwhile to investigate various molecules, especially macromolecules such as fluorescent proteins. Also, the establishment of a method to load sperm cells with various molecules, such as a more accomplished single-cell electroporation technique, is still needed.

## SUPPORTING MATERIAL

Three figures are available at http://www.biophysj.org/biophysj/supplemental/S0006-3495(10)00052-4.

The authors thank H. Abe and Y. Oka at the University of Tokyo for their assistance with single-cell electroporation, and the staff members at both the Misaki Marine Biological Station at the University of Tokyo and the Marine and Costal Research Center at Ochanomizu University, as well as to Mr. F. Matsuzawa (Fumi-Maru, Manazuru, Kanagawa, Japan) for supplying the sea urchins.

This work was supported by a Grant-in-Aid for Exploratory Research (20657014) and Grants-in-Aid for Scientific Research on Priority Areas (1704911, 19037010) from The Ministry of Education, Culture, Sports, Science and Technology of Japan, as well as by the Creation and Application of Soft Nano-Machine, the Hyperfunctional Molecular Machine program.

## REFERENCES

1. Tombes, R. M., C. J. Brokaw, and B. M. Shapiro. 1987. Creatine kinase-dependent energy transport in sea urchin spermatozoa. *Biophys. J.* 52:75–86.
2. Takao, D., and S. Kamimura. 2008. FRAP analysis of molecular diffusion inside sea-urchin spermatozoa. *J. Exp. Biol.* 211:3594–3600.
3. Pesch, S., and M. Bergmann. 2006. Structure of mammalian spermatozoa in respect to viability, fertility and cryopreservation. *Micron.* 37:597–612.
4. Mitchell, B. F., L. B. Pedersen, …, D. R. Mitchell. 2005. ATP production in *Chlamydomonas reinhardtii* flagella by glycolytic enzymes. *Mol. Biol. Cell.* 16:4509–4518.
5. James, P. S., C. Hennessy, …, R. Jones. 2004. Compartmentalization of the sperm plasma membrane: a FRAP, FLIP and SPFI analysis of putative diffusion barriers on the sperm head. *J. Cell Sci.* 117: 6485–6495.
6. Ladha, S., P. S. James, …, R. Jones. 1997. Lateral mobility of plasma membrane lipids in bull spermatozoa: heterogeneity between surface domains and rigidification following cell death. *J. Cell Sci.* 110:1041–1050.
7. Mackie, A. R., P. S. James, …, R. Jones. 2001. Diffusion barriers in ram and boar sperm plasma membranes: directionality of lipid diffusion across the posterior ring. *Biol. Reprod.* 64:113–119.
8. Rosenbaum, J. L., and G. B. Witman. 2002. Intraflagellar transport. *Natl. Rev.* 3:813–825.

9. Bisgrove, B. W., and H. J. Yost. 2006. The roles of cilia in developmental disorders and disease. *Development.* 133:4131–4143.

10. Berbari, N. F., A. K. O'Connor, …, B. K. Yoder. 2009. The primary cilium as a complex signaling center. *Curr. Biol.* 19:R526–R535.

11. Christensen, S. T., L. B. Pedersen, …, P. Satir. 2007. Sensory cilia and integration of signal transduction in human health and disease. *Traffic.* 8:97–109.

12. Swezey, R. R., and D. Epel. 1989. Stable, resealable pores formed in sea urchin eggs by electric discharge (electroporation) permit substrate loading for assay of enzymes in vivo. *Cell Regul.* 1:65–74.

13. Takao, D., and S. Kamimura. 2010. Single-cell electroporation of fluorescence probes into sea urchin sperm cells and FRAP analysis. *Zoolog. Sci.* 27:279–284.

14. Bestman, J. E., R. C. Ewald, …, H. T. Cline. 2006. In vivo single-cell electroporation for transfer of DNA and macromolecules. *Nat. Protoc.* 1:1267–1272.

15. Fall, C. P., E. S. Marland, …, J. J. Tyson (eds.). 2002. Interdisciplinary Applied Mathematics 20: Computational Cell Biology, 1st ed. Springer-Verlag, New York, NY.

16. Axelrod, D., D. E. Koppel, …, W. W. Webb. 1976. Mobility measurement by analysis of fluorescence photobleaching recovery kinetics. *Biophys. J.* 16:1055–1069.

17. Ladha, S., A. R. Mackie, and D. C. Clark. 1994. Cheek cell membrane fluidity measured by fluorescence recovery after photobleaching and steady-state fluorescence anisotropy. *J. Membr. Biol.* 142:223–228.

18. Yguerabide, J., J. A. Schmidt, and E. E. Yguerabide. 1982. Lateral mobility in membranes as detected by fluorescence recovery after photobleaching. *Biophys. J.* 40:69–75.

19. Satir, P. 1968. Studies on cilia. 3. Further studies on the cilium tip and a ''sliding filament'' model of ciliary motility. *J. Cell Biol.* 39:77–94.

20. Nicastro, D., J. R. McIntosh, and W. Baumeister. 2005. 3D structure of eukaryotic flagella in a quiescent state revealed by cryo-electron tomography. *Proc. Natl. Acad. Sci. USA.* 102:15889–15894.

21. Deane, J. A., D. G. Cole, …, J. L. Rosenbaum. 2001. Localization of intraflagellar transport protein IFT52 identifies basal body transitional fibers as the docking site for IFT particles. *Curr. Biol.* 11:1586–1590.

22. Corbit, K. C., P. Aanstad, …, J. F. Reiter. 2005. Vertebrate smoothened functions at the primary cilium. *Nature.* 437:1018–1021.

23. Marshall, W. F., and S. Nonaka. 2006. Cilia: tuning in to the cell's antenna. *Curr. Biol.* 16:R604–R614.

24. Praetorius, H. A., and K. R. Spring. 2001. Bending the MDCK cell primary cilium increases intracellular calcium. *J. Membr. Biol.* 184:71–79.

25. Nauli, S. M., F. J. Alenghat, …, J. Zhou. 2003. Polycystins 1 and 2 mediate mechanosensation in the primary cilium of kidney cells. *Nat. Genet.* 33:129–137.